HHS Public Access

Author manuscript

Cell Rep. Author manuscript; available in PMC 2023 October 23.

Published in final edited form as:

Cell Rep. 2023 February 28; 42(2): 112087. doi:10.1016/j.celrep.2023.112087.

The cellular basis of mechanosensation in mammalian tongue

Yalda Moayedi[1,2,3], **Shan Xu**[4], **Sophie K. Obayashi**[5], **Benjamin U. Hoffman**[1], **Gregory J. Gerling**[4,*], **Ellen A. Lumpkin**[1,5,6,*]

[1]Department of Physiology and Cellular Biophysics, Columbia University, New York, NY 10032, USA

[2]Department of Neurology, Columbia University, New York, NY 10032, USA

[3]Department of Otolaryngology – Head & Neck Surgery, Columbia University, New York, NY 10032, USA

[4]School of Engineering and Applied Science, University of Virginia, Charlottesville, VA 22904, USA

[5]Department of Molecular & Cell Biology, Helen Wills Neuroscience Institute, University of California, Berkeley, Berkeley, CA 94720, USA

[6]Lead contact

SUMMARY

Mechanosensory neurons that innervate the tongue provide essential information to guide feeding, speech, and social grooming. We use *in vivo* calcium imaging of mouse trigeminal ganglion neurons to identify functional groups of mechanosensory neurons innervating the anterior tongue. These sensory neurons respond to thermal and mechanical stimulation. Analysis of neuronal activity patterns reveal that most mechanosensory trigeminal neurons are tuned to detect moving stimuli across the tongue. Using an unbiased, multilayer hierarchical clustering approach to classify pressure-evoked activity based on temporal response dynamics, we identify five functional classes of mechanosensory neurons with distinct force-response relations and adaptation profiles. These populations are tuned to detect different features of touch. Molecular markers of functionally distinct clusters are identified by analyzing cluster representation in genetically marked neuronal subsets. Collectively, these studies provide a platform for defining

*Correspondence: gg7h@virginia.edu (G.J.G.), lumpkin@berkeley.edu (E.A.L.).

AUTHOR CONTRIBUTIONS

All authors gave final approval and agree to be accountable for all aspects of the work. E.A.L. supervised experimental studies and G.J.G. supervised clustering analysis. Conceptualization, Y.M. and E.A.L.; methodology, Y.M., B.U.H., S.X., S.K.O., G.J.G., and E.A.L.; formal analysis, Y.M., S.X., S.K.O., G.J.G., and E.A.L.; investigation, Y.M.; resources, E.A.L., Y.M., and G.J.G.; data curation, Y.M., E.A.L., and G.J.G.; writing – original draft, Y.M.; writing – review and editing, Y.M., B.U.H., S.X., S.K.O., G.J.G., and E.A.L.; visualization, Y.M., S.X., and S.K.O.; supervision, E.A.L. and G.J.G.; project administration, E.A.L.; funding acquisition, E.A.L., G.J.G., and Y.M.

DECLARATION OF INTERESTS

The authors declare no competing interests.

SUPPLEMENTAL INFORMATION

Supplemental information can be found online at https://doi.org/10.1016/j.celrep.2023.112087.

INCLUSION AND DIVERSITY

We support inclusive, diverse, and equitable conduct of research. Received: April 12, 2022

the contributions of functionally distinct mechanosensory neurons to oral behaviors crucial for survival in mammals.

In brief

The tongue, which is among our most touch-sensitive organs, needs sensory information to guide feeding, speech, and social behaviors. Moayedi et al. use *in vivo* calcium imaging and computational clustering to identify five types of mechanosensory neurons innervating the anterior tongue. Most are tuned to detect moving stimuli, thereby facilitating active tasks.

Graphical abstract

The graphical abstract was created with BioRender.com.

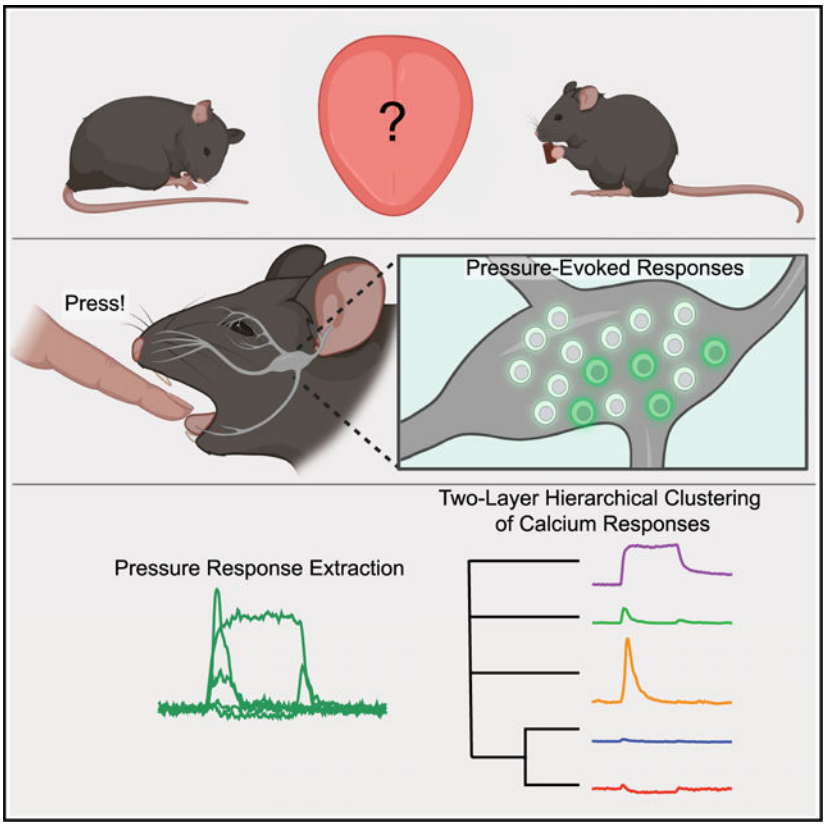

INTRODUCTION

Trigeminal sensory neurons innervating the oral cavity provide essential sensory feedback during myriad survival and social behaviors. For example, during feeding, somatosensory neurons encode thermal, chemical, and textural features of foodstuffs, which signal freshness and nutrient content.[1–5] To chew and swallow without injury, animals rely on mechanosensory neurons embedded in oral and upper airway mucosa.[6–9] Mechanosensory neurons in the oral cavity are equally important for social exchange that promotes species survival. During speech, mechanosensory neurons in the tongue and hard palate provide

sensory inputs needed to produce vowels and sibilants.[10–12] Furthermore, somatosensory neurons innervating the tongue are important for social bonding, such as maternal licking behavior and allogrooming in rodents.[13–16]

Despite these essential functions, only a handful of studies have interrogated the neural substrates of somatosensation in the tongue. The trigeminal ganglion encompasses a rich diversity of chemo-, thermo-, and mechanoreceptors. Most studies have focused on mechanisms of thermal and chemosensation in the oral cavity, which are relevant to both feeding and oral pain.[17–26] By contrast, few studies have specifically analyzed mechanosensory responses of lingual trigeminal neurons.[27–30] This is particularly important, as the tip of the tongue is exquisitely mechanosensitive with acuity comparable with that of the fingertip.[31,32] In previous studies, we reported the neurochemistry and morphology of peripheral neurons innervating the tongue in mice and humans, including mechanosensory axons in fungiform and filiform papillae that express the mechanically gated ion channel Piezo2.[33,34] The anatomy of these neurons is distinct from Piezo2-positive afferents in skin and other tissues; therefore, their functions in sensation are unknown. Previous electrophysiological studies identified functionally distinct neurons innervating the mammalian tongue.[23–25,30,35–37] In humans and cats, most tongue mechanoreceptors are rapidly adapting, a property typical of Meissner corpuscles, indicating that the tongue is tuned for detection of moving stimuli.[23,35–38] In addition, mouse geniculate ganglion mechanoreceptors selectively respond to moving stimuli and not to static pressure.[39] Open questions remain about whether the tongue is innervated by distinct types of mechanoreceptors capable of encoding diverse tactile qualities, whether rare neuronal groups are present, and whether mechanosensory neurons are molecularly distinguishable.

Here we use *in vivo* calcium imaging to investigate the functional and molecular properties of tongue-innervating trigeminal ganglion neurons. We developed a hierarchical clustering approach to classify temporal response patterns of mechanosensory neurons, which provides an unbiased method to perform calcium imaging analysis. Furthermore, we identified two rare groups of mechanosensory neurons that have not been previously described in mice.

RESULTS

To analyze tongue-innervating trigeminal neurons, we adapted methods for *in vivo* calcium imaging of the trigeminal ganglion.[17] Previous studies have shown that trigeminal neurons have robust responses to cold stimulation of the oral cavity.[17,18] Thus, we first tested whether tongue-innervating neurons displayed cooling- or pressure-evoked calcium responses using mice that express GCaMP6f in all trigeminal cells (*Wnt1*^{Cre};*Rosa26*^{Ai95}). The tongue was gently extended and stabilized on a platform, allowing stimulation of the tongue independent of other oral structures and facial skin (Figure 1A). We applied five discrete mechanical stimuli using a force-controlled indenter (0.09–0.44 N, corresponding to 29–140 kPa). Next, room-temperature (RT) water followed by ice-cold water was flowed across the tongue (Figure 1B). Individual neurons responded to pressure or flowing liquid or were polymodal with both pressure- and flow-evoked responses (Figures 1C and 1D; Video S1). Pooled data from hundreds of neurons show that distinct subsets of neurons respond to RT or cold flowing water, pressure, and both stimulus modalities (Figure 1E). The majority

of responding neurons were RT/cold flow sensitive (83%, Figure 1F). These neurons tended to respond to both RT and cold flow stimuli, with greater response magnitude for cold stimulation compared with RT, consistent with previous studies of oral thermoreceptors.[17,18] Approximately 17% of responsive trigeminal neurons were pressure sensitive (Figures 1E and 1F). Of these, fewer than half selectively responded to pressure. The remaining neurons were polymodal, responding both to pressure and RT/cold flow, as previously reported for cats.[23,35] By comparing the somatal sizes of functionally distinct groups, we found that trigeminal neurons that were selectively activated by mechanical stimuli were significantly larger than both the RT/cold flow-responsive neurons and polymodal neurons (Figure 1G). Collectively, these data demonstrate that tongue-innervating trigeminal neurons include distinct classes of thermosensory, mechanosensory, and polymodal neurons.

Oral behaviors, such as feeding, vocalization, and grooming, involve tongue movements that cause fluctuations in force across the mucosal surface; therefore, we posited that the rodent tongue might be equipped with mechanoreceptors tuned to detect moving stimuli. To test this hypothesis, we compared the responses of tongue mechanosensory neurons to sustained pressure and to dynamic brush stimulation (Figure 2). Almost all neurons (95%) were brush sensitive. Of these, 72% responded only to brush and 23% responded to both brush and pressure. The remaining 5% of neurons responded selectively to pressure stimuli (Figures 2B–2E; Video S2). These data are in excellent agreement with previous electrophysiological studies from cat lingual afferents and mouse cutaneous afferents.[23,35,40] Among pressure-responsive neurons, we noticed that neurons responded with subjectively different decay kinetics; neurons that responded selectively to pressure tended to do so with sustained calcium increases throughout the stimulus duration, whereas brush- and pressure-responsive neurons tended to show transient increases in fluorescence. Moreover, brush-selective neurons had significantly smaller somata than pressure-selective neurons (Figure 2F). Thus, as in the skin, the tongue is innervated by multiple classes of mechanosensory neurons with distinct somatal diameters, temporal response patterns to pressure, and sensitivity to submodalities of touch.

In skin, genetic markers label subsets of mechanoreceptors with different functional properties; therefore, we screened transgenic Cre mouse lines that label cutaneous low-threshold mechanoreceptors to determine whether they also mark tongue-innervating trigeminal mechanoreceptors. Cre lines were chosen that mark subsets of mechanosensory neurons in the skin in an effort to identify a broad range of genetically tractable mechanosensory neurons. Cre-driver lines were crossed with mouse reporter lines that express membrane-bound GFP.[41,42] We found that trigeminal ganglion neurons were labeled with three different Cre markers (Figures 3A–3C): the GDNF (glial cell line-derived neurotrophic factor) receptor Ret (*Ret*^{CreERT2} tamoxifen-induced at postnatal day 21 [P21] to P30), vesicular glutamate transporter 3 (*Vglut3*^{Cre}), and the NT-3 receptor *Ntrk3*^{CreERT2} (tamoxifen-induced at P21–P30).[40,43–46] By quantifying marker expression in trigeminal ganglia, we found that *Ret*^{CreERT2} labeled 31%, *Vglut3*^{Cre} labeled 29%, and *Ntrk3*^{CreERT2} labeled 10% of trigeminal neurons. In tongue, each of these genetic markers labeled afferents that innervated filiform and fungiform papilla (Figure S1). Thus, these genetic marker strains identify afferents that innervate the anterior tongue's principal sensory appendages.

Cre lines were then used to drive GCaMP6f expression in subsets of trigeminal neurons for *in vivo* calcium imaging. Ret^{+} neurons encompassed brush-, pressure- and brush/pressure-sensitive subsets of mechanosensory neurons (Figure 3D). During sustained pressure, distinct temporal response patterns were also observed, with most neurons showing transient responses and a rare subset showing sustained responses. *Vglut3*-lineage neurons were also pressure/brush sensitive, but they lacked sustained responses to pressure (Figure 3E). Ntrk3-expressing neurons were also sensitive to both pressure and brushing; pressure responses were a mixture of both sustained and transient types (Figure 3F). By contrast, $Ntrk2^{CreERT2}$, which marks a subset of rapidly adapting dorsal root ganglion (DRG) neurons, and $Parv^{Cre}$, which labels DRG proprioceptors, showed no responses in trigeminal ganglia when the tongue was mechanically stimulated.[41,47] These data are consistent with previous reports demonstrating very few Ntrk2-positive trigeminal neurons innervating the tongue and that the cell bodies of proprioceptors that innervate oral regions reside in the mesencephalic nucleus rather than the trigeminal ganglion.[29,48,49] Collectively, our results show that lingual mechanosensory neurons across molecular subtypes preferentially encode dynamic mechanical stimuli.

Although distinct temporal response patterns to pressure were observed, they did not correlate with the transgenic markers tested. Thus, we sought an objective method to determine how many distinct groups of mechanosensory neurons innervate the tongue. Somatosensory neurons are typically grouped based on their responses to discrete stimulus modalities (e.g., thermal, mechanical, noxious) or through subjective categorization of response dynamics (e.g., transient, sustained). These subjective grouping schemes are prone to experimenter bias and can fail when neurons exhibit intermediate response properties or when rare populations exist. Thus, we developed a scheme for unbiased clustering of mechanoreceptor responses to pressure. Data were combined from all mechanosensory neurons in $Ret^{CreERT2}$, $Vglut3^{Cre}$, and $Ntrk3^{CreERT2}$ lines and blinded to mitigate experimenter bias. Time-series data were preprocessed before clustering, which included noise removal, baseline drift correction, peak detection, normalization to peak, and interstimulus interval removal (Figure 4A). We tested both partitioning and hierarchical clustering methods. Results from partitioning clustering were not stable across different runs. Partitioning clustering also failed to distinguish subtle differences observed in traces with low-amplitude responses, as described below. By contrast, hierarchical clustering results were constant across repeated runs. Among multiple linkage criteria tested, Ward1 criterion resulted in the clear separation of unique clusters. We then applied a second iteration of clustering to each primary cluster to examine whether additional groups were distinguishable. In this round, traces were only denoised and baseline corrected, which allowed for clustering based on information such as response amplitude and direction (Figure 4A). Initial hierarchical clustering identified four clusters (*Cl*) with distinct temporal patterns (Figure 4B). When *Cl1*, *Cl2*, and *Cl3* were individually analyzed in a nested clustering round, response patterns of subclusters were indistinguishable within each cluster. By contrast, *Cl4* separated into four subclusters. Surprisingly, force steps reduced fluorescence in two of these subclusters. Thus, we separated *Cl4* into a group with little or no fluorescence change (*Cl4a*) and one that showed fluorescence reductions during force steps (*Cl4b*). Overall, our hierarchical clustering approach identified five functional

groups of tongue-innervating mechanosensory neurons with differences in response kinetics, amplitude, and valence.

We next quantitatively analyzed the response properties of neurons in each cluster (*Cl1–4b*, Figure 5). Clusters were unequally represented across the population, ranging from 4.5% to 43.3% of mechanosensory neurons (Figure 5A). Clusters displayed differences in mean amplitudes and temporal kinetics in response to the highest force level tested (Figure 5B) as well as median soma size (Figure 5C). These results demonstrate that biological differences within the population of tongue-innervating mechanosensory neurons were captured in the clustering approach.

Cl1 neurons (4.5%) showed large, sustained fluorescence increases during force steps but weak responses to brush stimuli (Figures 5D–5D‴). We noted that these neurons had significantly larger somata than all other clusters (Figure 5C). Analysis of force-response curves showed that force magnitude positively correlated with the activity of *Cl1* neurons at both the initial peak and steady state (Figure 5D‴′). Comparison of linear fits between peak and steady-state responses show that their slopes did not differ significantly. Thus, *Cl1* neurons, likely slowly adapting touch receptors, encode force magnitude throughout the duration of pressure stimuli.

By contrast, *Cl2* neurons, which were the most abundant class in this study (43%), showed small, transient “on” responses at all force levels tested and were robustly activated by brush (Figures 5E–5E‴). Some of these neurons also showed “off” responses, which were generally smaller than “on” responses. *Cl2* peak responses had a slightly positive slope to increasing forces, indicating that these neurons only weakly represent stimulus magnitude in their neuronal activity (Figure 5E‴′). Steady-state response amplitudes were near baseline, suggesting that these neruons adapt to force. Together, these data indicate that individual *Cl2* neurons, like rapidly adapting mechanoreceptors, are tuned to detect dynamic stimuli but do not represent stimulus magnitude.

Cl3 neurons (9%) also showed transient responses to pressure steps; however, their stimulus-response relations were markedly different from those of other clusters. Peak fluorescence signals were similar among the low and intermediate forces tested, but these neurons exhibited large response amplitudes at 0.44 N (Figures 5F–5F‴). Thus, this cluster showed a steep positive slope in peak force-response relations (Figure 5F‴′). Moreover, they responded more vigorously to force steps than to brush. These response properties suggest that *Cl3* neurons are high-threshold mechanoreceptors that respond preferentially to noxious mechanical stimuli.

Conversely, *Cl4a* neurons (38%) showed little or no calcium increases during force steps but responded vigorously to brush (Figures 5G–5G‴). Neurons in this cluster had a slightly positive initial force-response relation and were silent at steady state (Figure 5G‴′). Thus, *Cl4a* neurons are brush receptors. *Cl4b* neurons (5%) showed similar brush sensitivity and very small fluorescence increases at the onset of force steps (Figures 5H–5H‴). Unexpectedly, these neurons showed sustained fluorescence decreases at the highest force levels tested. Although the initial positive response showed a stimulus-response slope of

zero, the magnitude of the steady-state response was negatively correlated with force amplitude (Figure 5H‴′). This surprising result indicates that a small population of tongue mechanoreceptors is progressively inhibited by increasing pressures but robustly activated by brush.

We next compared the distribution of neurons derived from each Cre line in the full dataset with the distribution of genetic markers in each cluster to determine whether these molecular markers distinguish functionally defined neuronal classes (Figure 6). *Cl1*, which responded best to force steps, comprised *Ntrk3*- or *Ret*-expressing neurons, with only 1 out of 28 neurons of *Vglut3* lineage. The distribution of molecular markers in this cluster differed significantly from that of the population as a whole. These data are consistent with expression of *Ret* and *Ntrk3* in cutaneous slowly adapting mechanoreceptors.[40,46,50] *Cl2*, which showed transient responses at all forces, contained neurons from all three genetic marker strains at proportions similar to that of the parent population. *Cl3* neurons, which are putative mechanonociceptors, comprised 89% *Vglut3*-lineage neurons, 11% *Ret*-expressing neurons, and no *Ntrk3*-expressing neurons. These data are consistent with known expression of Ret in high-threshold mechanoreceptors.[45,46] By contrast, to our knowledge *Vglut3*-lineage neurons have not been previously implicated in mechanonociception.[45,46] *Cl4a* neurons included all three molecular markers, and the distribution was comparable with the population as a whole. *Cl4b* contained almost entirely *Vglut3*-lineage or *Ntrk3*-expressing neurons, with only one Ret^{+} neuron. This distribution was particularly surprising because Ret is widely expressed in adult mechanosensory neurons. In summary, the overlap in response properties between Cre-driver lines suggests that these genetic markers label overlapping but distinct subsets of trigeminal mechanosensory neurons.

DISCUSSION

Although tongue-innervating sensory neurons play a critical role in flavor, feeding, and social behaviors, the diversity of mechanosensory neurons innervating the tongue has not been systematically analyzed. Here, we combined a panel of genetic reporter mouse strains, *in vivo* trigeminal calcium imaging of hundreds of neurons in parallel, and a custom *in silico* clustering paradigm. We found that most lingual mechanosensory neurons are tuned for dynamic stimuli: they are brush sensitive and show transient responses to sustained pressure. This representation makes sense given the complex trajectories of the tongue during chewing, speech, and other oral tasks. Moreover, we identified five distinct classes of mechanosensory neuronal subsets that differ in prevalence, cell-body size, force-response relationships, and decay kinetics. Finally, our results indicate that trigeminal tongue-innervating mechanoreceptors achieve response profiles similar to those of cutaneous afferents, despite their divergent end-organ morphologies.[33]

Functional classes of tongue-innervating trigeminal mechanoreceptors

We identified functionally distinct subsets of trigeminal tongue-innervating mechanosensory neurons using an unbiased hierarchical clustering approach. Clustering response dynamics using a multilayer hierarchical approach offered significant advantages over the manual classification typically used in calcium imaging analysis including speed, objectivity

of results, and identification of rare groups. In all, we identified five types of tongue-innervating mechanosensory neurons based on their response profiles to ramp-and-hold pressure. The results demonstrate that trigeminal mechanosensory tongue-innervating neurons are capable of transducing a broad range of mechanical stimuli including dynamic brush and innocuous to noxious pressure. This is in stark contrast to previous reports of geniculate mechanoreceptors, which have been shown to respond only to moving stimuli.[39]

Only one cluster, *Cl1*, was preferentially activated by pressure compared with brush stimulation. This was the least frequent subtype observed and included sustained responding neurons that encoded pressure across the full range of stimuli tested. These sustained response patterns are similar to slowly adapting responses recorded from cutaneous sensory neurons. Similar to such slowly adapting neurons, *Cl1* neurons had the largest cell diameters in our sample. In skin, these responses are produced by Merkel cell-neurite complexes and possibly Ruffini endings;[51,52] however, neither of these end-organ types have been identified in mouse tongue.[33] Moreover, this cluster was only weakly brush sensitive, whereas Merkel cell afferents are robustly activated by laterally moving stimuli.[53] Thus, additional studies are needed to identify the end organs in tongue that give rise to these rare and sustained responses.

Cl2, the largest cluster, comprised brush-sensitive neurons that showed transient response to pressure at stimulus onset and, often, stimulus offset. These response characteristics match those of rapidly adapting responses common for Meissner's and Pacinian corpuscles.[38] Although Meissner's and Pacinian corpuscles are not present in the rodent tongue, our previous studies identified PIEZO2-positive end bulbs of Krause, which are afferent terminals encased in Nestin-positive Schwann cells within filiform papillae.[33] The high frequency of this end-organ type in the mouse tongue is in agreement with abundance of *Cl2* neurons, indicating that the filiform papillae encapsulated endings might be the source of the transient *Cl2* response.

Cl3 neurons also displayed transient responses to stimulation, with little activation at low forces and large responses at the highest force ranges tested. These force-response relations resemble high-threshold mechanoreceptors.[54] This population had the second smallest somatic cell diameters, which suggests that this cluster consists of either Aδ mechanonociceptors or C-nociceptors. It is possible that these neurons form free nerve endings, such as those previously identified in both the filiform and fungiform papillae of mice.[33]

Cl4a neurons were also brush sensitive but showed little or no response to pressure. This response profile is similar to that of field receptors, which are stroke-sensitive neurons identified in cat and mouse hairy skin.[40] In mice, field receptors form circumferential endings that wrap around hair follicles. A correlate in mouse tongue has not been observed.

The final cluster, *Cl4b*, displayed transient increase in activity due to pressure followed by a sustained force-encoding inhibition. This response type could signify a spontaneously active neuron that has a transient increase in activity at high forces, followed by inhibition. The expression of mechanically gated, two-pore potassium channels has been documented

in the trigeminal ganglia; such expression in a constitutively active neuron could result in mechanically induced inhibition of firing.[55] *Cl4b* was also highly brush sensitive and had the smallest soma size of all clusters.

Functionally identified tongue trigeminal mechanoreceptors are conserved across mammals

Three of the mechanosensory tongue-innervating trigeminal neuron clusters identified in this study are likely to be conserved with those identified previously in humans and cats.[23,35–37] In humans, four low-threshold mechanosensory neuron groups have been described using microneurography of the lingual nerve.[36,37] These included rapidly adapting units, slowly adapting units with regular firing, slowly adapting units with irregular firing, and deep mechanoreceptors with proprioceptive capabilities. Similar populations were identified in cats.[23,35] Like cluster *Cl1* neurons, slowly adapting mechanoreceptors were the smallest response group identified in humans and cats. Our study did not identify two clusters of sustained responding neurons, as the temporal resolution of our calcium imaging approach did not suffice in detecting single action potentials. The majority of tongue-innervating neurons identified in humans and cats were rapidly adapting,[35–37] in agreement with our findings that *Cl2* was the most abundant cluster in mouse tongue. In cats, an additional population of neurons was identified that was responsive to brushing but not pressure, similar to *Cl4a* in our study.

We also noted some differences between our findings and previous electrophysiological studies of tongue trigeminal mechanoreceptors. This study identified two clusters, *Cl3* and *Cl4b*, for which correlates have not been identified in humans or cats. We were surprised to observe that *Cl4b* neurons showed mechanically evoked decreases in intracellular calcium. Such responses are consistent with inhibitory activity, which, to our knowledge, has not been reported for trigeminal neurons. In prior work in humans, the force stimulation range was subthreshold to nociceptors; thus, the methods used were not optimal for identifying high-threshold mechanoreceptors such as those of *Cl3*.[36,37] Furthermore, caveats of the methods used in human studies cited by the authors include a bias toward large-diameter neurons and spontaneously active neurons, collectively leading to potential undersampling of high-threshold mechanoreceptors. In keeping with this notion, *Cl3* and *Cl4b* had the smallest somal diameters of all clusters identified in this study. In addition, owing to the relatively small sample size that is feasible to achieve with microneurography, rare neuronal subtypes might not have been captured. Although proprioceptors have been previously reported in human lingual nerve recordings,[37] they were not analyzed in our studies because trigeminal ganglia do not contain the somata of cranial proprioceptors. Finally, one previous study recorded pressure-response dynamics in mechanosensory neurons using *ex vivo* tongue-nerve preparations from a mouse oral cancer model.[30] This study found that high-threshold mechanoreceptors were the most abundant class present in the tongue and that most lingual mechanoreceptors are slowly adapting. The intriguing differences in the results of the latter study and those presented here could be due to sensitization resulting from injection of human cells in the tongue, strain differences between athymic nude mice and immunocompetent animals, or differences in recording methods.

Tongue-innervating mechanoreceptors are functionally and molecularly conserved but anatomically distinct from cutaneous mechanoreceptors

Mapping of molecular markers to lingual mechanosensory neuron groups reveals insights into how these functional classes compare with skin-innervating mechanoreceptors. *Ret* is expressed in around 60% of DRG neurons including non-peptidergic nociceptors, Meissner corpuscles, Pacinian corpuscles, and lanceolate endings.[46] In oral tissues, *Ret* is expressed in tooth pulp afferents[56] and in geniculate ganglion neurons innervating fungiform papillae.[19] Only one cluster, *Cl4b*, did not include *Ret* -positive cells. Thus, molecular identification of this cluster can be performed through transcriptomic analysis of *Ret* mechanoreceptors in the trigeminal ganglion in future studies. VGLUT3 has previously been shown to be expressed transiently in Merkel cell afferents and persistently in both C-low-threshold mechanoreceptors (LTMRs) and a class of unmyelinated free nerve endings innervating skin.[45] In lingual mechanoreceptors, *Vglut3*-lineage neurons were predominantly included in *Cl2–4b*. These include neurons with properties of transient LTMRs (*Cl2*), high-threshold mechanoreceptors (*Cl3*), brush-responsive neurons (*Cl4a*), and neurons with a reduction in cytoplasmic calcium during noxious stimulation (*Cl4b*). These data suggest that the tongue has distinct but overlapping functional diversification of mechanosensory *Vglut3*-lineage neuron types compared with skin-innervating mechanoreceptors. *Ntrk3* is expressed in Merkel cell afferents, Aβ field LTMRs, and a subset of free nerve endings.[40] In adults, around half of adult TrkC-positive DRG neurons are also *Ret* positive. Accordingly, we found that *Ntrk3*-expressing neurons were present in all lingual clusters except *Cl3*, the high-threshold mechanoreceptor group. Collectively, this strategy identified three clusters that were distinguishable by the absence of a molecular marker. In future studies, transcriptomic and intersectional genetic approaches can be used to definitively identify and manipulate these neuronal clusters to analyze their contributions to lingual mechanosensation.

Our findings differ from those of a previous report of the molecular identities of tongue-innervating trigeminal neurons.[29] The latter study concluded that small proportions of trigeminal ganglia neurons that innervate the tongue are marked by $Parv^{Cre}$ and $TrkB^{CreERT2}$, whereas our analysis of these genetic markers identified no mechanosensory neurons in tongue. Our methods would only identify mechanosensory neurons with receptive fields within the locations of stimulation; thus, it is possible that these neurons identified in previous studies are not mechanosensory or they have receptive fields in different locations in the tongue. Additionally, the prior study found minimal *Vglut3* RNA expression in tongue-innervating neurons. VGLUT3 is known to have transient expression in subpopulations of low-threshold mechanosensory neurons during development.[45] It is possible that the populations we have identified as tongue-innervating mechanoreceptors may not have persistent expression, and express GCaMP due to transient developmental expression of VGLUT3.

In the tongue, peripheral mechanosensory end organs have distinct morphologies compared with those of known mechanoreceptors of the skin, making inferences of how endings relate to function speculative. We sought to identify whether specific end organs correlated with any of the genetic markers that we investigated in this work. We found that neuronal

afferents from all three transgenic Cre lines were present in both the filiform and fungiform papillae. Further complicating this quest to identify end organs associated with the populations reported in this study is that fungiform papillae are also innervated by geniculate neurons, some of which express *Ret* and *Ntrk3*.[19,57] To the best of our knowledge, expression of *Vglut3*-lineage neurons has not been investigated in the geniculate ganglion. Thus, future studies will need to disentangle whether molecularly labeled mechanosensory end organs in the fungiform papillae are derived from trigeminal or geniculate ganglia.

Contributions of tongue mechanoreceptors to oral sensation and behavior

Previous studies of the contributions of sensation to tongue function have focused heavily on the roles of geniculate and trigeminal chemoreceptors in flavor perception and nutrient acquisition; however, this study highlights the rich array of mechanoreceptors that are poised to provide sensory feedback during diverse oral cavity functions, including mastication, vocalization, and grooming. During chewing and bolus formation, the tongue presses food against the hard palate, which activates pressure-sensitive receptors. This pressure sensation not only helps to signal the position of food and the tongue in the mouth but might also play a role in evaluating liquid viscosity and other flavor features.[58,59] Merkel cells of the hard palate are likely to be involved in this pressure coding, whereas tongue *Cl1* neurons are well poised to detect fluctuations in force during chewing.[33,60] During drinking and feeding, liquids also flow across the surface of the tongue. This flow is likely to be encoded by the transient and brush-sensitive neurons (*Cl2*, *Cl4a*, and *Cl4b*).

These transiently active and brush-sensitive neurons are also likely to play multiple roles in social behaviors. During speech, neurons that are tuned to detect movement (*Cl2*, *Cl4a*, *Cl4b*) at the tongue's tip will provide feedback for phonemes with high-frequency components such as "s" and "t." In rodents and other species that perform social grooming, these neurons will report sensations that guide licking behaviors for conspecific social behaviors such as grooming and maternal licking.[13]

Finally, the tongue is exposed to painful high-force pressures, particularly during chewing, which help to alert the individual of inappropriate tongue coordination and protect against mechanical damage. *Cl3* are most likely a form of high-threshold mechanoreceptor that is capable of encoding these noxious pressures. In pathological states following trauma or inflammation, previously innocuous stimuli can also become noxious, resulting in mechanical hyperalgesia or allodynia. Mechanical hyperalgesia involves peripheral neuron hyperexcitability, decreased activation thresholds, and awakening of "silent" primary nociceptors, as well as central sensitization.[54,61] We surmise that *Cl3* may play a role in mechanical hypersensitivity and that other populations of mechanonociceptors exist that either had thresholds for activation higher than the force range that was presented or that require an inflammatory insult to be sensitized. Mechanical allodynia relies on sensory inputs from low-threshold mechanoreceptors in the cutaneous system.[54] Thus, it is possible that trigeminal populations identified in this study that are tuned for innocuous dynamic stimuli play roles in the development of mechanical allodynia. Future studies should more thoroughly examine nociceptive populations innervating the tongue and their roles in the generation of acute and chronic pain.

Collectively, we found that the majority of tongue-innervating mechanosensory neurons had transient responses to force and were brush sensitive, implying that the mouse tongue is best at encoding moving stimuli. This finding is consistent with those in humans and cats and is in line with a role for the tongue in active sensing during dynamic tasks such as feeding, speaking, and grooming.[23,35,37]

Limitations of the study

Several limitations should be kept in mind when interpreting the results of this study. First, the temporal resolution of our recordings by calcium imaging (10 Hz) is not sufficient to capture single action potentials; therefore, differences in neuronal firing rates between subpopulations could not be addressed. Second, although the pressure series applied in this study (29–140 kPa) ranges from normal pressures that the tongue experiences during feeding (up to 60 kPa) to noxious stimuli, additional pressure levels and dynamic stimulus modalities are experienced during active tongue movements.[62–64] Thus, future studies should address other stimulus modalities and pressure ranges to capture the complete population of high-threshold mechanoreceptors. Third, the proportions of mechanosensory subclasses might be skewed, as the transgenic Cre lines used here could have introduced sampling bias. Notably, we observed in our initial analysis that females have disproportionately fewer *Cl3* neurons but, as the number of neurons recorded from each sex is not balanced, we cannot make strong conclusions on sex-dependent differences. Future studies should rigorously address potential differences. Fourth, although our experimental strategy was designed to analyze most of the trigeminal mechanoreceptors innervating the anterior tongue, some minor populations were not sampled in this study. For example, the trigeminal ganglia comprise most of the somatosensory neurons innervating the tongue, but mechanoreceptors in the geniculate ganglia innervate fungiform papilla and neurons from the mesencephalic nucleus carry proprioceptive information. Moreover, imaging in this study was performed using wide-field fluorescent microscopy. While this afforded us the ability to image from a large population of neurons in the same field of view, it limited the imaging field to only the top layer of neurons in the trigeminal ganglia. Thus, we cannot be confident that all tongue-innervating neurons are imaged in a single experiment.

There are also some limitations arising from the preparation used to access the tongue in a living mouse. Because of technical restrictions in accessing the posterior tongue, only responses from the anterior tongue were recorded. Thus, additional neural populations might have receptive fields in the posterior tongue or cell bodies in the petrosal ganglia. Recordings from other sensory ganglia and posterior tongue are needed to survey these additional mechanoreceptive populations. Furthermore, the tongue is gently pulled and affixed to a platform for imaging; therefore, it is possible that the tension generated by pulling could affect mechanical responses. To mitigate this possibility, care was taken to ensure that the tongue remained pliable, and extension was minimized to avoid any tissue damage or inflammation. Stimulation was applied close to the tip of the tongue; thus, it is unlikely that extension of the back of the tongue would impact mechanoreceptors located at the tip. Finally, this initial characterization of tongue mechanoreceptors provides information on force-response properties of neuronal classes but does not provide information about

receptive field sizes of individual neuron classes or the relative distribution of receptive fields in the tongue (e.g., localization in the tip or margins). Future studies should address regional differences in mechanosensory innervation of the tongue.

STAR★METHODS

RESOURCE AVAILABILITY

Lead contact—Correspondence and requests for resources should be directed to the lead contact, Ellen A. Lumpkin (ellen.a.lumpkin@gmail.com).

Materials availability—This study did not generate new unique reagents.

Data and code availability

- All data reported in this paper is available from the lead contact upon request.
- All custom code has been deposited at Github and is publicly available as of the date of publication. DOIs are listed in the key resources table.
- Any additional information required to reanalyze the data reported in this paper is available from the lead contact upon request.

EXPERIMENTAL MODEL AND SUBJECT DETAILS

Animal assurance statement—All animal experiments were conducted in accordance with Columbia University's Animal Care and Use Policies. Mice were housed on a 12 h light/dark cycle with *ad libitum* food/water. Experiments were performed with male and female mice, 4–12 months old. Number of mice and sexes used are indicated in figure legends for each experiment. Cre lines were purchased from Jackson Labs or received from published authors, and crossed with reporter lines without additional backcrossing.

Mouse lines—Mouse lines used in this study included *Wnt1*^{Cre} (*129S4.Cg-E2f1*$^{Tg(Wnt1\text{-}cre)2Sor/J}$), *Ret*^{CreERT2} (*Ret*$^{tm2(cre/ERT2)Ddg}$), *Ntrk3*^{CreERT2} (*Ntrk3*$^{tm3.1(cre/ERT2)Ddg/J}$), *VGLUT3*^{Cre} (*Slc17a8*$^{tm1.1(cre)Hze}$), *Rosa26*^{Ai95} (*B6J.Cg-Gt*(*ROSA*)*26Sor*$^{tm95.1(CAG\text{-}GCaMP6f)Hze}$/*MwarJ*), *Rosa26*$^{mT/mG}$ (*B6.129*(*Cg*)*-Gt*(*ROSA*)*26Sort*$^{m4(ACTB\text{-}tdTomato,\text{-}EGFP)Luo/J}$), *Tau*^{eGFP} (*B6.Cg-Mapt*$^{tm1(EGFP)Klt\ Tg(MAPT)8cPdav/J}$).

METHOD DETAILS

Tamoxifen injections—For tamoxifen inducible lines, 150 mg/kg tamoxifen was injected intraperitoneally once between P21-P30. Tamoxifen was dissolved in 10% ethanol diluted in corn oil.

In vivo* imaging—In vivo* calcium imaging of tongue-innervating trigeminal neurons was conducted in anesthetized mice as previously described.[17] In brief, mice were deeply anesthetized with ketamine (100 mg/kg) and xylazine (10 mg/kg). The mouse was maintained at 37°C, and respiration was monitored for a steady rate within the normal effort range. Whiskers and hairs around the mouth were clipped to ensure that mechanical

stimuli did not unintentionally cause movement of hairs. Mice were head-fixed to a stable rod, tracheotomized, and hemispherectimized to expose the trigeminal ganglion. Once hemostasis was achieved, the ventral surface of the tongue was gently affixed to a platform with a spot of tissue glue and pulled out of the mouth. The tongue was monitored and adjusted to avoid swelling due to tension. Imaging was performed within 1 h of exposing the trigeminal ganglion. Brushing of the tongue was used to identify the region with the most abundant tongue-stimulation evoked responses. A force-controlled indenter (300C Dual Mode Muscle Lever; Aurora Scientific, Aurora, Canada) with a 2 mm tip was used to apply mechanical stimuli to the tongue. The force-controlled indenter was used as opposed to von Frey filaments as it allows for repeated application of forces to exactly the same position over successive trials, allowing for consistent stimulation of the same receptive fields within an experiment and consistent timing of stimulation between experiments. The mechanical stimuli applied ranged from 90 to 440 mN (29–140 kPa), which corresponds to ~0.2 mN–3.9 mN (or 0.02–0.4 g) von Frey filaments. Typically, we identified around 20 mechanosensory neurons per field of view using the 2 mm tip. The stimulator tip was placed near the tip of the tongue, with >4 mm distance from the face, ensuring that other regions of the face were not stimulated with pressure. Brushing was applied using a wire cell culture loop 10 times from posterior to anterior followed by 10 times from anterior to posterior. The region of brushing was visually targeted to the same region that the Aurora tip was placed and avoided the face. Cold and room temperature (RT) flow stimuli were applied to the tongue with a 1 mL handheld pipette without additional measures to avoid facial regions. Images were collected at 10 Hz using a Scientifica MultiPhoton In Vivo SliceScope equipped with an Olympus Plan N 4x (NA 0.10) lens. Illumination was provided by a CoolLED pE-300 (Andover, UK). Imaging was performed using Ocular (Teledyne Photometrics; Tucson, AZ). Image capture, LED shuttering, and pressure applications were synchronized using a Digidata 1550B (Molecular Devices; San Jose, CA).

In vivo imaging analysis—Motion correction was performed using NoRMCorre.[66] To assign Regions of Interest (ROIs), neurons were picked for analysis using the Cell Magic Wand plugin in ImageJ.[65] Image files were converted to ΔF using image subtraction, and neurons were chosen for subsequent analysis if they showed calcium fluctuations during any stimulation window. Out-of-focus neurons were excluded from analysis. Cell soma areas were calculated using the ROIs assigned in ImageJ.

For visualizing neural activity as heatmaps and for clustering analysis, neuropil extraction and ΔF/F calculation was performed using previously published modified MATLAB code with the median fluorescence for the entire trace used as F_0.[67] Custom MATLAB code was used to filter traces, identify peaks, remove spontaneously firing neurons, and assign to response group (e.g., pressure, brush). Traces were lowpass filtered using a fourth order polynomial, with passband frequency of 2, and passband ripple of 0.5. Filtered traces were then smoothed using a Savitzky-Golay filter function with a first order polynomial over a nine-sample span. Peaks were then identified using the find peaks function in MATLAB with a peak threshold of 1.5 ΔF/F. Peaks were aligned to stimulation windows with buffering time at the end of stimulus application to account for “off” responses. Neurons were defined as spontaneously firing and removed from analysis if the number of peaks outside of

the stimulation windows was greater than the number of peaks inside of the stimulation windows divided by half of the total number of peaks:

$$Spontaneous = peaks\ outside\ stimulation\ windows > \frac{peaks\ inside\ stimulation\ windows}{\frac{total\ peaks}{2}}$$

Response groups were assigned to neurons that had peaks within any of the relevant stimulation windows (e.g., pressure-responsive neurons had peaks only within a pressure stimulus window but not within a cold/cool or brush stimulus window).

Clustering analysis—Clustering analysis was performed to identify mechanosensory neuron subtypes based on their responses to pressure stimuli using R. Responses to pressure only were used for clustering analysis as these are location, timing, and pressure controlled and thus amenable to automated clustering analysis. The brushing stimuli were handheld so application position and speed were not matched across experimental animals. These differences between experiments in timing of brush application and force of brush applied introduces confounds that would bias the clustering toward neurons from the same experimental animal. Collected time-series ΔF/F traces from the neuropil extraction program for all cells were first cleaned before clustering. More specifically, the high-frequency noise was removed using the Butterworth low-pass filter with a frequency of 0.05. The baseline drift was corrected by deriving trends for intervals between pressure stimuli using the Butterworth low-pass filter with frequency of 0.005 and connecting inter-stimulus interval trends using spline interpolation. Responses to pressure stimuli were detected if they were above a threshold of twice the highest value among the first 60 s unstimulated period. To offset differences in fluorescence due to imaging sessions or inherent difference in GCaMP expression, detected responses of all cells were normalized to share the same highest value. As time intervals between two pressure stimuli was 50 s long, 40 s of each inter-stimulus interval was removed to condense signals to pressure responses only.

The preprocessed, neuropil extracted DF/F traces were clustered in a two-layer structure. In the first layer, hierarchical clustering was conducted using the Ward1 clustering linkage criterion and the Euclidean distance of Fourier coefficients as the distance measurement.[68,69] The number of clusters was determined by incrementally increasing from a small number until no clusters with unique patterns could be separated out. In the second layer, the same hierarchical clustering scheme was applied to each cluster obtained in the first layer to examine subclusters. In layer 2, de-noised and baseline corrected calcium traces without response detection and normalization were analyzed. Per first-layer cluster, if all subclusters in the second layer exhibited the same pattern, that first-layer cluster would be assigned as one individual neuron type. Otherwise, subclusters with unique response patterns would be separated from the first-layer cluster and assigned as different cluster types. In addition to the above multi-layer hierarchical clustering, singlelayer clustering and partitioning clustering were also tested for comparison.

Quantitative analysis of stimulus-response relations—Peak and steady-state values were analyzed using custom-written code in MATLAB. Mean gray value was extracted for

each ROI (as assigned above) to obtain raw fluorescence traces. To correct for bleaching, calcium imaging traces for each ROI were detrended by removing a second or third order polynomial trend [detrend() function in MATLAB]. Traces were separated into pressure and brush stimulus windows (frames 1 to 3550 and frames 3551 to 4680, respectively) for detrending. Following this step, traces were separated into stimulus-response windows by extracting the fluorescence values (F) from the 5 s prior to and the 20 s after stimulus onset (25 s total). The resulting traces were normalized to baseline (F_0), defined as the average fluorescence from the 5 s window prior to stimulus onset, and subsequently smoothed using a three-point moving average filter. Visualization and processing of stimulus-response traces were performed using modified MATLAB code.[70] Max peak was defined as the maximal change in normalized fluorescence (DF/F) from baseline within the first 3 s following stimulus onset. Steady-state peak values were calculated by averaging the normalized fluorescence during the last 2 s of stimulation.

Histology—Immunohistochemistry was performed as previously described.[33] Tongues were flash frozen in OCT (Tissue-Tek) in liquid nitrogen. Trigeminal ganglia were fixed in 4% paraformaldehyde for 2 h, washed in PBS, and submerged in 30% sucrose. Sagittal tissue cryosections (25 μm) were prepared on slides. Sections were dried at 37°C for 1 h, and tongue sections were post-fixed in 4% paraformaldehyde for 15 min. Slides were washed in PBS and incubated in 5% normal goat serum (NGS) + PBST (PBS, 0.3% Triton X-100) at room temperature for 1 h. Sections were then incubated overnight in primary antibody mixed in NGS + PBST at 4°C. The next day, slides were washed three times in PBST and then incubated for 2 h in secondary antibody mixed in NGS + PBST. Following this, slides were washed five times in PBS, and then mounted in Fluoromount-G with DAPI (Southern Biotech).

Antibodies used in this study were chicken anti-GFP (1:1000 Abcam, ab13970, lot GR236651–25, RRID:AB_300798), rabbit anti-β3 tubulin (1:3000, Abcam, ab18207, lot GR3221401–3, RRID:AB_444319), rat anti-keratin8 (1:100, Developmental Studies Hybridoma

Bank, supernatant, RRID:AB_531826), Alexa 488 anti-chicken (1:1000, ThermoFisher, A-11039, RRID:AB_2534096), Alexa 594 anti-rat (1:1000, Fisher Scientific, A11007, RRID:AB_141374), Alexa 647 anti-rabbit (1:1000, Fisher Scientific, A21244, RRID:AB_2535812).

Confocal microscopy—Histology was imaged using a Leica SP8 confocal microscope using LasX software. Images were taken with either a 10x NA = 0.40 air lens or 40x oil immersion lens with NA = 1.3. Images were taken at 2048×2048 pixels with 2x line averaging and Z-step size of 1 μm. Analysis was performed in ImageJ. Images were prepared for presentation in Adobe Photoshop by adjusting the threshold across the entire image.

Quantification of Cre + trigeminal neurons—Confocal images of trigeminal ganglia from each Cre line (N = 2–3 images/ganglion, 6 ganglia from 3 mice per strain) were analyzed for GFP expression. Images from a single ganglion were collected from sections

located at least 100 μm apart. For each genotype, images were acquired using the same confocal acquisition settings across all experiments. Neuron regions of interest were picked in ImageJ based on β3-tubulin expression and presence of a discernable nuclei. At least 200 neurons were counted from each ganglion. A 2-pixel Gaussian blur and threshold was applied to include the top 3% of pixels. Regions of interest in which the majority of pixels were GFP+ were counted as Cre + cells.

QUANTIFICATION AND STATISTICAL ANALYSIS

Statistical analysis—No statistical methods were used to predetermine sample sizes. Neurons were excluded from analysis if they were out of focus, showed spontaneous activity (defined above), or had no responses to stimulation. Animals were excluded from analysis if they had no responses to stimulation. Max peak and average steady-state fluorescence ΔF/F values were calculated in MATLAB. Graph-Pad Prism 9 was used for graph visualization and statistical analysis. Data were tested for normality and either a One-way ANOVA with Tukey's post hoc or a Kruskal Wallis test with Dunn's multiple comparisons was applied as appropriate. Categorical data were analyzed with Chi square tests. Linear regressions were used to assess differences in force-response curves. Statistical details for each experiment are included in figure legends or figures including test type, n, what n represents, p values, and dispersion and precision intervals. Significance levels are *$p < 0.05$, **$p < 0.01$, ***$p < 0.001$, ****$p < 0.0001$.

Supplementary Material

Refer to Web version on PubMed Central for supplementary material.

ACKNOWLEDGMENTS

We thank Drs. David Ginty and Meenakshi Rao for providing $Ret^{CreERT2}$ mice, Dr. David Yarmolinsky for training on trigeminal imaging procedures, and Drs. Alexander Chesler and Marcin Szczot for providing neuropil extraction code. We thank Dr. Rachel Clary and members of the SENse Lab at University of California, Berkeley for helpful discussions. This work was supported by the Berrie Foundation Initiative on the Neurobiology of Obesity (E.A.L. and Y.M.), the Thompson Family Foundation Initiative on Chemotherapy Induced Peripheral Neuropathy and Sensory Neuroscience (Y.M. and E.A.L.), NIH NINDS R01NS105241 (G.J.G. and E.A.L.), and NIH NIDCD R21DC018898 (Y.M.).

REFERENCES

1. Canon F, Belloir C, Bourillot E, Brignot H, Briand L, Feron G, Lesniewska E, Nivet C, Septier C, Schwartz M, et al. (2021). Perspectives on astringency sensation: an alternative hypothesis on the molecular origin of astringency. J. Agric. Food Chem 69, 3822–3826. 10.1021/acs.jafc.0c07474. [PubMed: 33682421]
2. Klein AH (2019). The orotrigeminal system. Handb. Clin. Neurol 164, 205–216. 10.1016/B978-0-444-63855-7.00013-7. [PubMed: 31604548]
3. Lemon CH (2017). Modulation of taste processing by temperature. Am. J. Physiol. Regul. Integr. Comp. Physiol 313, R305–R321. 10.1152/ajpregu.00089.2017. [PubMed: 28794101]
4. Schöbel N, Radtke D, Kyereme J, Wollmann N, Cichy A, Obst K, Kallweit K, Kletke O, Minovi A, Dazert S, et al. (2014). Astringency is a trigeminal sensation that involves the activation of G protein-coupled signaling by phenolic compounds. Chem. Senses 39, 471–487. 10.1093/chemse/bju014. [PubMed: 24718416]

5. Yu T, Shah BP, Hansen DR, Park-York M, and Gilbertson TA (2012). Activation of oral trigeminal neurons by fatty acids is dependent upon intracellular calcium. Pflugers Arch. 464, 227–237. 10.1007/s00424-012-1116-9. [PubMed: 22644615]
6. Inoue T, Kato T, Masuda Y, Nakamura T, Kawamura Y, and Morimoto T. (1989). Modifications of masticatory behavior after trigeminal deafferentation in the rabbit. Exp. Brain Res 74, 579–591. 10.1007/BF00247360. [PubMed: 2707333]
7. Moore JD, Kleinfeld D, and Wang F. (2014). How the brainstem controls orofacial behaviors comprised of rhythmic actions. Trends Neurosci. 37, 370–380. 10.1016/j.tins.2014.05.001. [PubMed: 24890196]
8. Thexton AJ, Hiiemae KM, and Crompton AW (1980). Food consistency and bite size as regulators of jaw movement during feeding in the cat. J. Neurophysiol 44, 456–474. 10.1152/jn.1980.44.3.456. [PubMed: 7441310]
9. Travers JB, and Norgren R. (1986). Electromyographic analysis of the ingestion and rejection of sapid stimuli in the rat. Behav. Neurosci 100, 544–555. 10.1037//0735-7044.100.4.544. [PubMed: 3741605]
10. Hickok G. (2012). Computational neuroanatomy of speech production. Nat. Rev. Neurosci 13, 135–145. 10.1038/nrn3158. [PubMed: 22218206]
11. Niemi M, Laaksonen JP, Ojala S, Aaltonen O, and Happonen RP (2006). Effects of transitory lingual nerve impairment on speech: an acoustic study of sibilant sound/s. Int. J. Oral Maxillofac. Surg 35, 920–923. 10.1016/j.ijom.2006.06.002. [PubMed: 16889939]
12. Niemi M, Laaksonen JP, Vähätalo K, Tuomainen J, Aaltonen O, and Happonen RP (2002). Effects of transitory lingual nerve impairment on speech: an acoustic study of vowel sounds. J. Oral Maxillofac. Surg 60, 647–652. 10.1053/joms.2002.33113. [PubMed: 12022101]
13. Stern JM, and Johnson SK (1989). Perioral somatosensory determinants of nursing behavior in Norway rats (Rattus norvegicus). J. Comp. Psychol 103, 269–280. 10.1037/0735-7036.103.3.269. [PubMed: 2776423]
14. Schweinfurth MK, Stieger B, and Taborsky M. (2017). Experimental evidence for reciprocity in allogrooming among wild-type Norway rats. Sci. Rep 7, 4010. 10.1038/s41598-017-03841-3. [PubMed: 28638051]
15. Stopka P, and Graciasová R. (2001). Conditional allogrooming in the herb-field mouse. Behav. Ecol 12, 584–589. 10.1093/beheco/12.5.584.
16. Wu YE, Dang J, Kingsbury L, Zhang M, Sun F, Hu RK, and Hong W. (2021). Neural control of affiliative touch in prosocial interaction. Nature 599, 262–267. 10.1038/s41586-021-03962-w. [PubMed: 34646019]
17. Yarmolinsky DA, Peng Y, Pogorzala LA, Rutlin M, Hoon MA, and Zuker CS (2016). Coding and plasticity in the mammalian thermosensory system. Neuron 92, 1079–1092. 10.1016/j.neuron.2016.10.021. [PubMed: 27840000]
18. Leijon SCM, Neves AF, Breza JM, Simon SA, Chaudhari N, and Roper SD (2019). Oral thermosensing by murine trigeminal neurons: modulation by capsaicin, menthol and mustard oil. J. Physiol 597, 2045–2061. 10.1113/JP277385. [PubMed: 30656684]
19. Donnelly CR, Shah AA, Mistretta CM, Bradley RM, and Pierchala BA (2018). Biphasic functions for the GDNF-Ret signaling pathway in chemosensory neuron development and diversification. Proc. Natl. Acad. Sci. USA 115, E516–E525. 10.1073/pnas.1708838115. [PubMed: 29282324]
20. Dickman JD, Colton JS, Chiszar D, and Colton CA (1987). Trigeminal responses to thermal stimulation of the oral cavity in rattlesnakes (Crotalus viridis) before and after bilateral anesthetization of the facial pit organs. Brain Res. 400, 365–370. 10.1016/0006-8993(87)90636-6. [PubMed: 3815082]
21. Poulos DA, and Lende RA (1970). Response of trigeminal ganglion neurons to thermal stimulation of oral-facial regions. II. Temperature change response. J. Neurophysiol 33, 518–526. 10.1152/jn.1970.33.4.518. [PubMed: 4988213]
22. Poulos DA, and Lende RA (1970). Response of trigeminal ganglion neurons to thermal stimulation of oral-facial regions. I. Steady-state response. J. Neurophysiol 33, 508–517. 10.1152/jn.1970.33.4.508. [PubMed: 4988212]

23. Robinson PP (1992). The effect of injury on the properties of afferent fibres in the lingual nerve. Br. J. Oral Maxillofac. Surg 30, 39–45. 10.1016/0266-4356(92)90135-6. [PubMed: 1550804]
24. Smith KG, and Robinson PP (1995). An experimental study of lingual nerve repair using epineurial sutures or entubulation. Br. J. Oral Maxillofac. Surg 33, 211–219. 10.1016/0266-4356(95)90002-0. [PubMed: 8736745]
25. Wang Y, Erickson RP, and Simon SA (1993). Selectivity of lingual nerve fibers to chemical stimuli. J. Gen. Physiol 101, 843–866. 10.1085/jgp.101.6.843. [PubMed: 8331321]
26. Lundy RF, and Contreras RJ (1995). Tongue adaptation temperature influences lingual nerve responses to thermal and menthol stimulation. Brain Res. 676, 169–177. 10.1016/0006-8993(95)00105-Y. [PubMed: 7796166]
27. Nguyen MQ, Wu Y, Bonilla LS, von Buchholtz LJ, and Ryba NJP (2017). Diversity amongst trigeminal neurons revealed by high throughput single cell sequencing. PLoS One 12, e0185543. 10.1371/journal.pone.0185543.
28. Nguyen MQ, Le Pichon CE, and Ryba N. (2019). Stereotyped transcriptomic transformation of somatosensory neurons in response to injury. Elife 8, e49679. 10.7554/eLife.49679.
29. Wu P, Arris D, Grayson M, Hung CN, and Ruparel S. (2018). Characterization of sensory neuronal subtypes innervating mouse tongue. PLoS One 13, e0207069. 10.1371/journal.pone.0207069.
30. Grayson M, Furr A, and Ruparel S. (2019). Depiction of oral tumor-induced trigeminal afferent responses using single-fiber electrophysiology. Sci. Rep 9, 4574. 10.1038/s41598-019-39824-9. [PubMed: 30872649]
31. Miles BL, Van Simaeys K, Whitecotton M, and Simons CT (2018). Comparative tactile sensitivity of the fingertip and apical tongue using complex and pure tactile tasks. Physiol. Behav 194, 515–521. 10.1016/j.physbeh.2018.07.002. [PubMed: 29981764]
32. Van Boven RW, and Johnson KO (1994). The limit of tactile spatial resolution in humans: grating orientation discrimination at the lip, tongue, and finger. Neurology 44, 2361–2366. 10.1212/wnl.44.12.2361. [PubMed: 7991127]
33. Moayedi Y, Duenas-Bianchi LF, and Lumpkin EA (2018). Somatosensory innervation of the oral mucosa of adult and aging mice. Sci. Rep 8, 9975. 10.1038/s41598-018-28195-2. [PubMed: 29967482]
34. Moayedi Y, Michlig S, Park M, Koch A, and Lumpkin EA (2021). Somatosensory innervation of healthy human oral tissues. J. Comp. Neurol 529, 3046–3061. 10.1002/cne.25148. [PubMed: 33786834]
35. Biedenbach MA, and Chan KY (1971). Tongue mechanoreceptors: comparison of afferent fibers in the lingual nerve and chorda tympani. Brain Res. 35, 584–588. 10.1016/0006-8993(71)90507-5. [PubMed: 5135555]
36. Trulsson M, and Essick GK (2010). Sensations evoked by microstimulation of single mechanoreceptive afferents innervating the human face and mouth. J. Neurophysiol 103, 1741–1747. 10.1152/jn.01146.2009. [PubMed: 20130037]
37. Trulsson M, and Essick GK (1997). Low-threshold mechanoreceptive afferents in the human lingual nerve. J. Neurophysiol 77, 737–748. 10.1152/jn.1997.77.2.737. [PubMed: 9065846]
38. Mountcastle VB, Talbot WH, Darian-Smith I, and Kornhuber HH (1967). Neural basis of the sense of flutter-vibration. Science 155, 597–600. 10.1126/science.155.3762.597. [PubMed: 4959494]
39. Yokota Y, and Bradley RM (2017). Geniculate ganglion neurons are multimodal and variable in receptive field characteristics. Neuroscience 367, 147–158. 10.1016/j.neuroscience.2017.10.032. [PubMed: 29097269]
40. Bai L, Lehnert BP, Liu J, Neubarth NL, Dickendesher TL, Nwe PH, Cassidy C, Woodbury CJ, and Ginty DD (2015). Genetic identification of an expansive mechanoreceptor sensitive to skin stroking. Cell 163, 1783–1795. 10.1016/j.cell.2015.11.060. [PubMed: 26687362]
41. Hippenmeyer S, Vrieseling E, Sigrist M, Portmann T, Laengle C, Ladle DR, and Arber S. (2005). A developmental switch in the response of DRG neurons to ETS transcription factor signaling. PLoS Biol. 3, e159. 10.1371/journal.pbio.0030159. [PubMed: 15836427]
42. Muzumdar MD, Tasic B, Miyamichi K, Li L, and Luo L. (2007). A global double-fluorescent Cre reporter mouse. Genesis 45, 593–605. 10.1002/dvg.20335. [PubMed: 17868096]

43. Griffith TN, Docter TA, and Lumpkin EA (2019). Tetrodotoxin-sensitive sodium channels mediate action potential firing and excitability in menthol-sensitive Vglut3-lineage sensory neurons. J. Neurosci 39, 7086–7101. 10.1523/JNEUROSCI.2817-18.2019. [PubMed: 31300524]
44. Grimes WN, Seal RP, Oesch N, Edwards RH, and Diamond JS (2011). Genetic targeting and physiological features of VGLUT3+ amacrine cells. Vis. Neurosci 28, 381–392. 10.1017/S0952523811000290. [PubMed: 21864449]
45. Lou S, Duan B, Vong L, Lowell BB, and Ma Q. (2013). Runx1 controls terminal morphology and mechanosensitivity of VGLUT3-expressing C-mechanoreceptors. J. Neurosci 33, 870–882. 10.1523/JNEUROSCI.3942-12.2013. [PubMed: 23325226]
46. Luo W, Enomoto H, Rice FL, Milbrandt J, and Ginty DD (2009). Molecular identification of rapidly adapting mechanoreceptors and their developmental dependence on ret signaling. Neuron 64, 841–856. 10.1016/j.neuron.2009.11.003. [PubMed: 20064391]
47. Rutlin M, Ho CY, Abraira VE, Cassidy C, Bai L, Woodbury CJ, and Ginty DD (2014). The cellular and molecular basis of direction selectivity of Aδ-LTMRs. Cell 159, 1640–1651. 10.1016/j.cell.2014.11.038. [PubMed: 25525881]
48. Huang T, Ohman LC, Clements AV, Whiddon ZD, and Krimm RF (2021). Variable branching characteristics of peripheral taste neurons indicates differential convergence. J. Neurosci 41, 4850–4866. 10.1523/JNEUROSCI.1935-20.2021. [PubMed: 33875572]
49. Lazarov NE (2007). Neurobiology of orofacial proprioception. Brain Res. Rev 56, 362–383. 10.1016/j.brainresrev.2007.08.009. [PubMed: 17915334]
50. Fünfschilling U, Ng YG, Zang K, Miyazaki JI, Reichardt LF, and Rice FL (2004). TrkC kinase expression in distinct subsets of cutaneous trigeminal innervation and nonneuronal cells. J. Comp. Neurol 480, 392–414. 10.1002/cne.20359. [PubMed: 15558783]
51. Johnson KO, Yoshioka T, and Vega-Bermudez F. (2000). Tactile functions of mechanoreceptive afferents innervating the hand. J. Clin. Neurophysiol 17, 539–558. 10.1097/00004691-200011000-00002. [PubMed: 11151974]
52. Iggo A, and Muir AR (1969). The structure and function of a slowly adapting touch corpuscle in hairy skin. J. Physiol 200, 763–796. 10.1113/jphysiol.1969.sp008721. [PubMed: 4974746]
53. Johnson KO, and Lamb GD (1981). Neural mechanisms of spatial tactile discrimination: neural patterns evoked by braille-like dot patterns in the monkey. J. Physiol 310, 117–144. 10.1113/jphysiol.1981.sp013540. [PubMed: 7230030]
54. Hill RZ, and Bautista DM (2020). Getting in touch with mechanical pain mechanisms. Trends Neurosci. 43, 311–325. 10.1016/j.tins.2020.03.004. [PubMed: 32353335]
55. Yamamoto Y, Hatakeyama T, and Taniguchi K. (2009). Immunohistochemical colocalization of TREK-1, TREK-2 and TRAAK with TRP channels in the trigeminal ganglion cells. Neurosci. Lett 454, 129–133. 10.1016/j.neulet.2009.02.069. [PubMed: 19429069]
56. Donnelly CR, Shah AA, Suh EB, and Pierchala BA (2019). Ret signaling is required for tooth pulp innervation during organogenesis. J. Dent. Res 98, 705–712. 10.1177/0022034519837971. [PubMed: 30958726]
57. Matsumoto I, Emori Y, Ninomiya Y, and Abe K. (2001). A comparative study of three cranial sensory ganglia projecting into the oral cavity: in situ hybridization analyses of neurotrophin receptors and thermosensitive cation channels. Brain Res. Mol. Brain Res 93, 105–112. 10.1016/s0169-328x(01)00129-2. [PubMed: 11589988]
58. Deblais A, Hollander ED, Boucon C, Blok AE, Veltkamp B, Voudouris P, Versluis P, Kim HJ, Mellema M, Stieger M, et al. (2021). Predicting thickness perception of liquid food products from their non-Newtonian rheology. Nat. Commun 12, 6328. 10.1038/s41467-021-26687-w. [PubMed: 34732723]
59. Miles BL, Wu Z, Kennedy KS, Zhao K, and Simons CT (2022). Elucidation of a lingual detection mechanism for high-viscosity solutions in humans. Food Funct. 13, 64–75. 10.1039/d1fo02460d. [PubMed: 34874045]
60. Nunzi MG, Pisarek A, and Mugnaini E. (2004). Merkel cells, corpuscular nerve endings and free nerve endings in the mouse palatine mucosa express three subtypes of vesicular glutamate transporters. J. Neurocytol 33, 359–376. 10.1023/B:NEUR.0000044196.45602.92. [PubMed: 15475690]

61. Pace MC, Passavanti MB, De Nardis L, Bosco F, Sansone P, Pota V, Barbarisi M, Palagiano A, Iannotti FA, Panza E, and Aurilio C. (2018). Nociceptor plasticity: a closer look. J. Cell. Physiol 233, 2824–2838. 10.1002/jcp.25993. [PubMed: 28488779]

62. Hori K, Ono T, and Nokubi T. (2006). Coordination of tongue pressure and jaw movement in mastication. J. Dent. Res 85, 187–191. 10.1177/154405910608500214. [PubMed: 16434740]

63. Yokoyama S, Hori K, Tamine K.i., Fujiwara S, Inoue M, Maeda Y, Funami T, Ishihara S, and Ono T. (2014). Tongue pressure modulation for initial gel consistency in a different oral strategy. PLoS One 9, e91920. 10.1371/journal.pone.0091920.

64. Hayashi H, Hori K, Taniguchi H, Nakamura Y, Tsujimura T, Ono T, and Inoue M. (2013). Biomechanics of human tongue movement during bolus compression and swallowing. J. Oral Sci 55, 191–198. 10.2334/josnusd.55.191. [PubMed: 24042584]

65. Schindelin J, Arganda-Carreras I, Frise E, Kaynig V, Longair M, Pietzsch T, Preibisch S, Rueden C, Saalfeld S, Schmid B, et al. (2012). Fiji: an open-source platform for biological-image analysis. Nat. Methods 9, 676–682. 10.1038/nmeth.2019. [PubMed: 22743772]

66. Pnevmatikakis EA, and Giovannucci A. (2017). NoRMCorre: an online algorithm for piecewise rigid motion correction of calcium imaging data. J. Neurosci. Methods 291, 83–94. 10.1016/j.jneumeth.2017.07.031. [PubMed: 28782629]

67. Ghitani N, Barik A, Szczot M, Thompson JH, Li C, Le Pichon CE, Krashes MJ, and Chesler AT (2017). Specialized mechanosensory nociceptors mediating rapid responses to hair pull. Neuron 95, 944–954.e4. 10.1016/j.neuron.2017.07.024. [PubMed: 28817806]

68. Murtagh F, and Legendre P. (2014). Ward's hierarchical agglomerative clustering method: which algorithms implement ward's criterion? J. Classif 31, 274–295. 10.1007/s00357-014-9161-z.

69. Mori U, Mendiburu A, and Lozano J. (2016). Distance measures for time series in R: the TSdist package. R J. 8, 451.

70. de Jong JW, Afjei SA, Pollak Dorocic I, Peck JR, Liu C, Kim CK, Tian L, Deisseroth K, and Lammel S. (2019). A neural circuit mechanism for encoding aversive stimuli in the mesolimbic dopamine system. Neuron 101, 133–151.e7. 10.1016/j.neuron.2018.11.005. [PubMed: 30503173]

Highlights

- Five functional subclasses of trigeminal mechanoreceptors innervate the mouse tongue
- Most tongue mechanosensory neurons are tuned to detect movement
- A small population of tongue-innervating mechanoreceptors encodes force magnitude
- Hierarchical clustering is a robust way to classify neurons based on calcium imaging

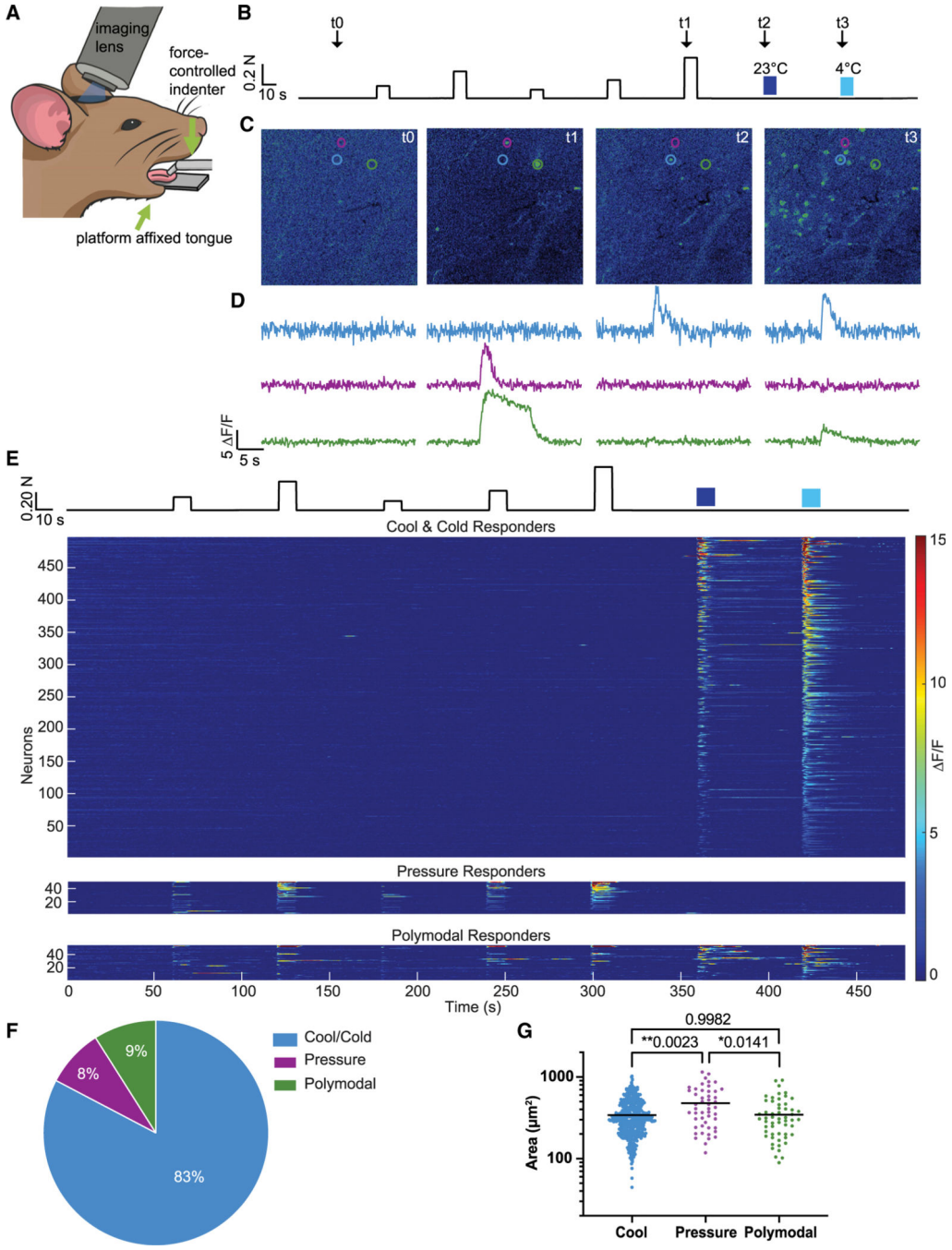

Figure 1. Somatosensory responses in tongue-innervating trigeminal neurons

(A) Mice were head-fixed, craniotomized, and brain-aspirated to reveal trigeminal ganglia. The tongue was affixed to a platform and gently pulled outward to mechanically isolate it from the rest of the oral cavity. A force-controlled indenter was used to stimulate the tongue on the ipsilateral side as the exposed trigeminal ganglion. Liquid stimuli were applied by hand to the tongue.

(B) Stimulation paradigm. Force-controlled indention was applied to the tongue between 0.09 N and 0.44 N. After 60 s, stimulations were applied for 10 s, followed by 50 s rest

before the next stimulation. Pressure was followed by room-temperature (RT) water (23°C) followed by cold water (4°C). Sample image times used in (C) are indicated by arrows (t0–t3).

(C) Sample images from baseline (t0), 0.40 N indention (t1), RT water (t2), and cold water (t3). Circled cells indicate neurons responsive to cool/cold flow only (blue), pressure only (purple), and pressure and cold (green).

(D) Traces from neurons in (C).

(E) Summary data from 601 neurons (n = 17 *Wnt1*^{Cre};*Rosa26*^{Ai95} mice, 7 male and 10 female). Neurons are separated into groups that responded to cool and/or cold only, pressure only, or both (polymodal).

(F) Distribution of neurons in each response category.

(G) Soma size was calculated for each neuron response class. Neurons responsive to pressure only were significantly larger than cool/cold or multimodal responders (Welch's ANOVA, p = 0.0029 with Dunnett's multiple comparisons, black bar denotes median). See also Video S1.

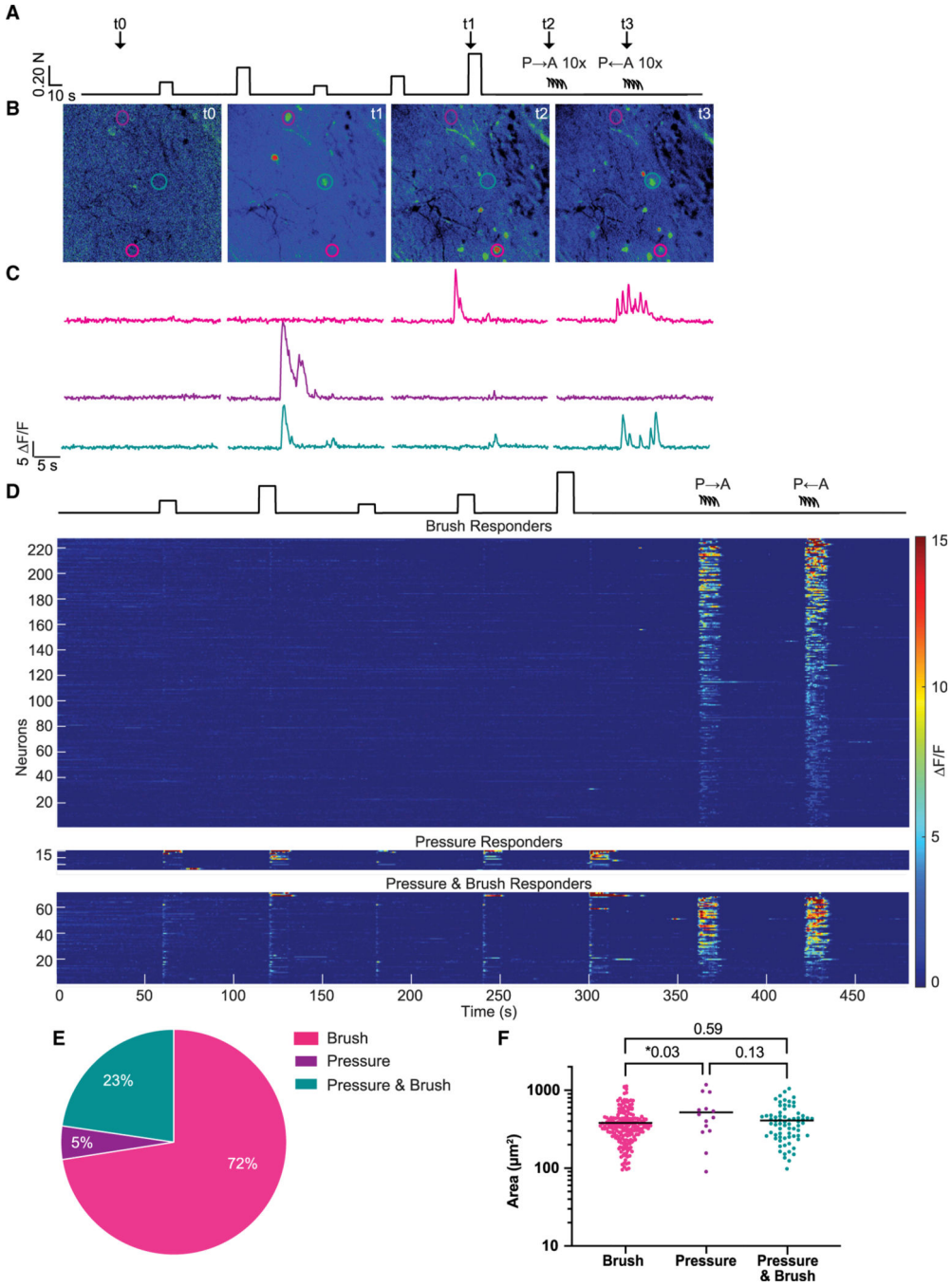

Figure 2. Tongue-innervating trigeminal mechanoreceptors are brush and/or pressure responsive

(A) Stimulus paradigm. Force-controlled indention was applied as in Figure 1 followed by 10 tongue brushes from posterior (P) to anterior (A), then A to P.

(B) Sample images are shown at baseline (t0), 0.4 N indention (t1), P-to-A brush (t2) and A-to-P brush (t3). Cells are circled that respond to brush only (pink), pressure only (purple), and pressure and brush (turquoise).

(C) Sample traces from neurons in (B).

(D) Summary data from 313 responding neurons from 13 *Wnt1*^{Cre};*Rosa26*^{Ai95} mice (7 male, 6 female).

(E) Distribution of neurons in each response category.

(F) Pressure-responsive neuron somas were significantly larger than brush-only responsive neurons (one-way ANOVA, p = 0.0346 with Tukey's post hoc test, black bar denotes median). See also Video S2.

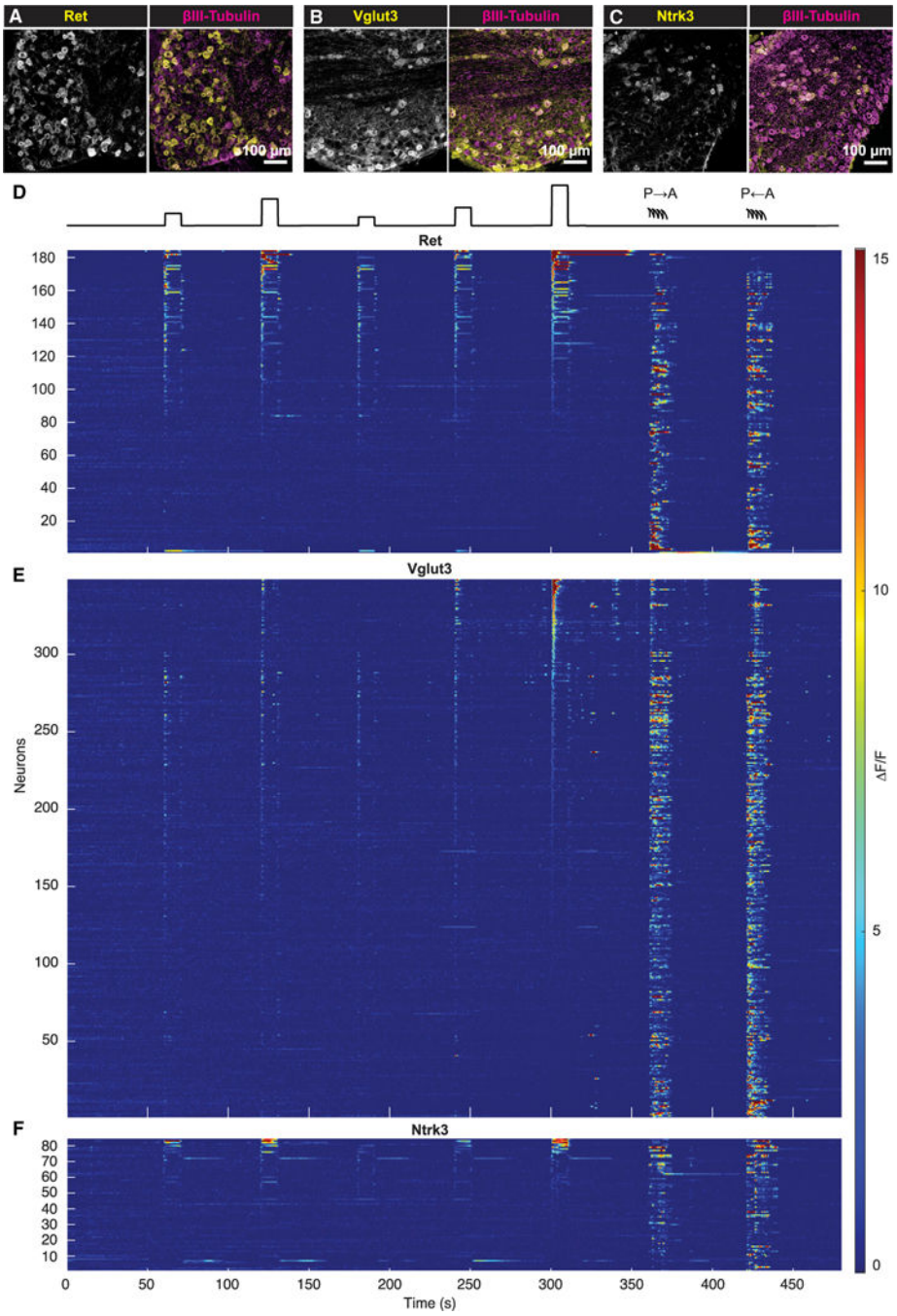

Figure 3. Tongue-innervating trigeminal mechanosensory neuron subgroups are distinguished by Cre lines

(A–C) Trigeminal ganglia of (A) *Ret*$^{CreERT2/+}$;*Rosa26*$^{mTmG/+}$, (B) *Vglut3*$^{Cre/+}$;*Rosa26*$^{TauGFP/+}$, and (C) *Ntrk3*$^{CreERT2/+}$;*Rosa26*$^{mTmG/+}$ animals reveal neuronal types marked by each line. Monochrome images on the left signify transgenic GFP expression in each Cre line, with β III-tubulin merge on the right. n = 6 ganglia from 3 mice/strain.

(D) *Ret*$^{+}$ tongue-innervating trigeminal mechanosensory neurons are both brush and pressure sensitive. Distinct response dynamics of pressure-sensitive neurons are apparent on heatmaps (total 184 neurons from 7 mice [4 male, 3 female]).
(E) *Vglut3*-lineage tongue-innervating trigeminal mechanosensory neurons are both brush sensitive and pressure sensitive. Pressure-sensitive neurons primarily show transient responses to pressure (348 neurons from 10 mice [5 male, 5 female]).
(F) *Ntrk3*$^{+}$ mechanosensory tongue-innervating trigeminal neurons are both pressure responsive and brush responsive. Pressure-responsive neurons show a variety of response dynamics apparent by heatmap (84 neurons from 7 mice [1 male, 6 females]).
See also Figure S1.

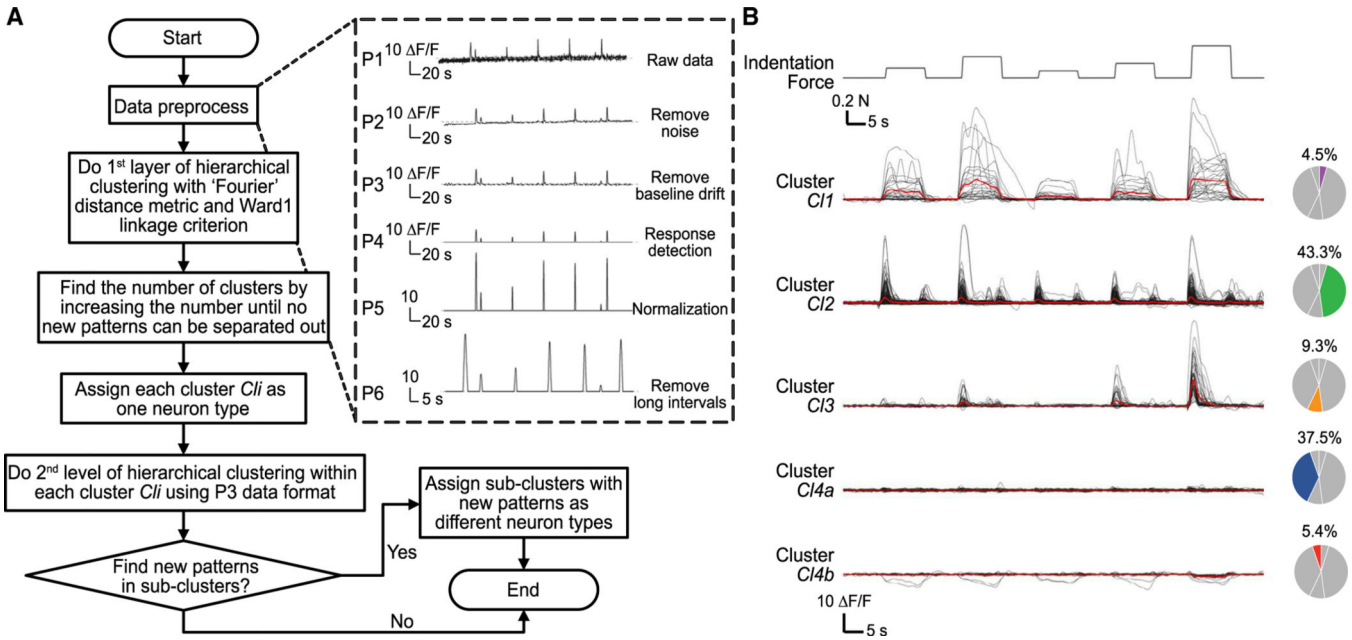

Figure 4. Hierarchical clustering approach to identify subpopulations of pressure-responsive neurons

(A) Logic diagram depicting steps for hierarchical clustering.

(B) Hierarchical clustering revealed four distinct clusters of response types in the first layer. Pressure responses from each group are shown with average response in red. Within cluster 4, a significant number of neurons showed a negative going response; thus, these were separated into a distinct cluster. Data are generated based on neurons recorded in Figure 3 (n = 616 neurons from 27 mice).

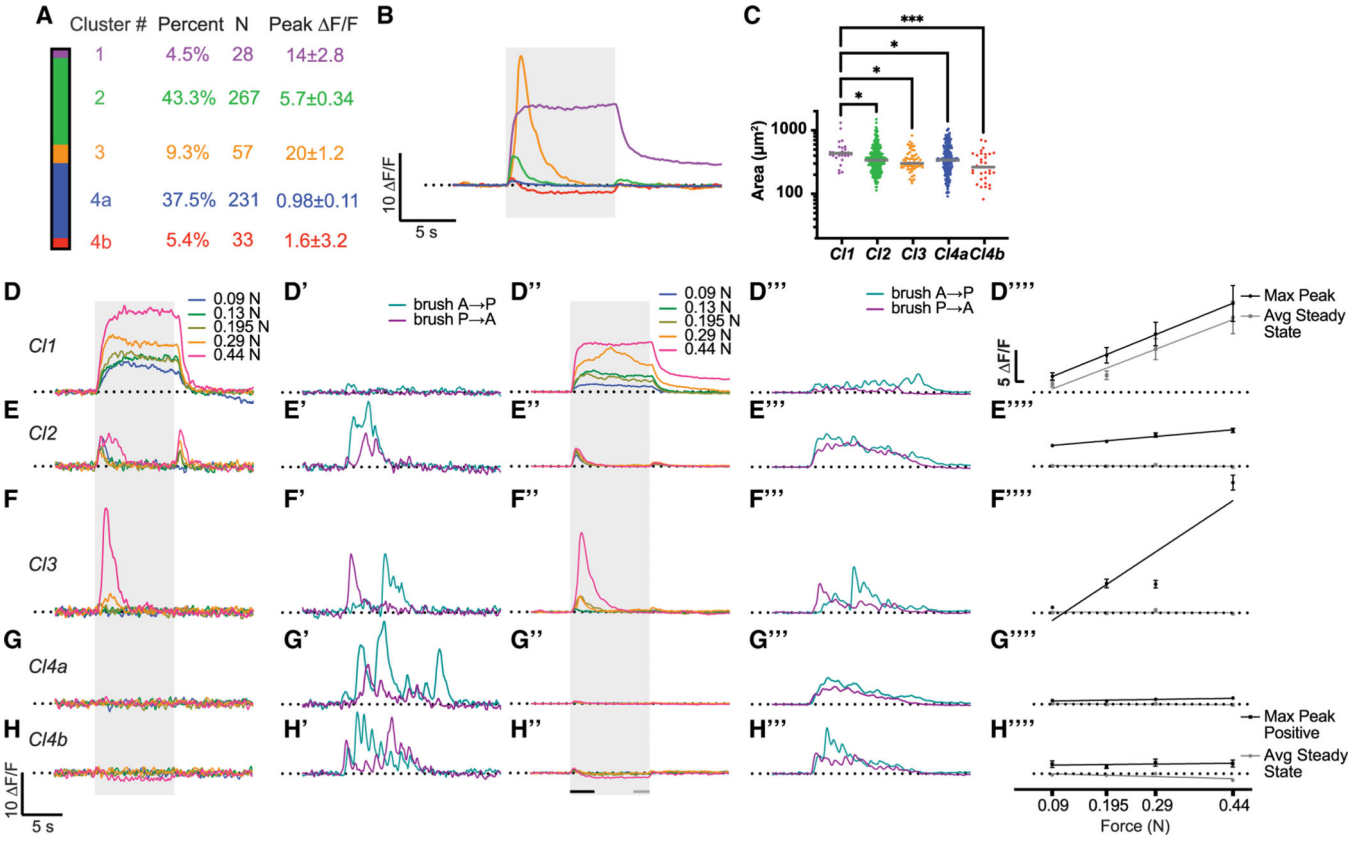

Figure 5. Clustering reveals five populations of tongue-innervating trigeminal mechanoreceptors with distinct response dynamics and cell-body sizes

(A) Percentage, number of neurons, and peak normalized change in fluorescence (ΔF/F) ± SEM are shown for each cluster. Data are generated based on clusters assigned in Figure 4 (n = 616 neurons from 27 mice).

(B) Average responses (ΔF/F) to maximum stimulation (0.44 N) for each cluster. Responses have subjectively distinguishable differences between magnitude and direction of response as well as kinetics of force response (shaded box indicates stimulation window).

(C) Cell areas for each cluster show that neuronal sizes are significantly different (Kruskal-Wallis test, $p = 0.0009$; Dunn's multiple comparisons, *$p < 0.05$, ***$p < 0.001$). *Cl1* consists of the largest-diameter neurons and *Cl4b* the smallest (gray bar denotes median).

(D–H) Representative responses to each force stimulation for each cluster (shaded box indicates pressure stimulation window: D, *Cl1*; E, *Cl2*; F, *Cl3*; G, *Cl4a*; H, *Cl4b*). (D′–H′) Representative responses to brushing from each cluster. (D″–H″) Average responses to force steps for each cluster. Bars below indicate stimulation windows from which maximum force responses (black) and average steady-state responses (gray) are calculated. (D‴–H‴) Average responses to brushing from each cluster. (D⁗–H⁗) Maximum response (black) from the first 3 s and average steady-state response (gray) from the last 2 s for each cluster are shown with linear fits to the population data. Dotted line denotes 0 ΔF/F. Mean ± SEM. (D⁗) Cluster 1. Maximum response to stimulation has a positive slope (slope = 0.33 (ΔF/F)/N, $R^2 = 0.17$, $p < 0.0001$). Steady-state response to stimulation has a similar positive slope (slope = 0.31 (ΔF/F)/N, $R^2 = 0.19$, $p < 0.0001$). Maximum and steady-state

slopes are not significantly different ($p = 0.8491$). (E‴′) Cluster 2. Maximum response to stimulation shows a slight positive slope (slope = 0.07 (ΔF/F)/N, $R^2 = 0.035$, $p < 0.0001$). Steady-state response to stimulation has a slight negative slope (slope = −0.0034 (ΔF/F)/N, $R^2 = 0.0055$, $p = 0.015$). Maximum and steady-state peaks are significantly different ($p < 0.0001$). (F‴′) Cluster 3. Maximum response to stimulation shows a positive slope (slope = 0.54 (ΔF/F)/N, $R^2 = 0.54$, $p < 0.0001$). Steady-state response to stimulation is not different from zero (slope = −0.0025 (ΔF/F)/N, $R^2 = 0.0034$, $p = 0.0056$). Maximum and steady-state peaks are significantly different ($p < 0.0001$). (G‴′) Cluster 4a. Maximum response to stimulation shows a slightly positive slope (slope = 0.012 (ΔF/F)/N, $R^2 = 0.015$, $p = 0.0002$). Steady-state response to stimulation has a slight negative slope (slope = −0.0046 (ΔF/F)/N, $R^2 = 0.043$, $p < 0.0001$). Maximum and steady-state peaks are significantly different ($p < 0.0001$). (H‴′) Cluster 4b. Maximum positive response to stimulation has a flat slope (slope = 0.008 (ΔF/F)/N, $R^2 = 0.0013$, $p = 0.68$). Steady-state response to stimulation has a slight negative slope (slope = −0.022 (ΔF/F)/N, $R^2 = 0.12$, $p < 0.0001$). Maximum and steady-state peaks are not significantly different ($p = 0.14$).

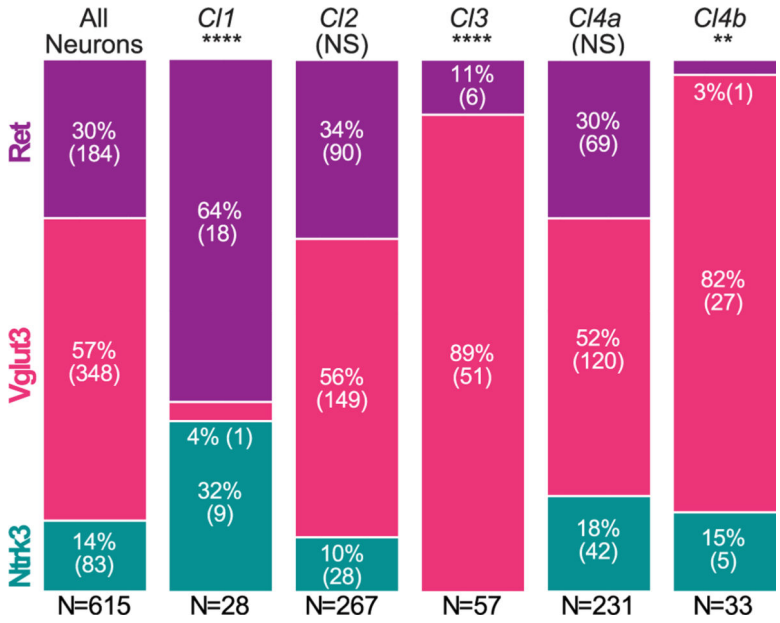

Figure 6. Molecular markers target clusters of tongue-innervating trigeminal mechanosensory neurons

Distribution of neurons from each Cre line are shown in each cluster. Data are generated based on clusters assigned in Figure 4 (n = 616 neurons from 27 mice). Chi-squared tests were performed with the number of neurons analyzed from each molecular marker as the expected distribution (**p < 0.01, ****p < 0.0001). *Cl1*, *Cl3*, and *Cl4b* had significantly different representations of Cre lines compared with neurons analyzed.

KEY RESOURCES TABLE

REAGENT or RESOURCE	SOURCE	IDENTIFIER
Antibodies		
chicken anti-GFP	Abcam	Cat#ab113970; RRID:AB_300798
rabbit anti-b3 tubulin	Abcam	Cat#ab18207; RRID:AB_444319
rat anti-keratin8	Developmental Studies Hybridoma Bank	Troma1; RRID:AB_531826
Alexa 488 anti-chicken	ThermoFisher	Cat#A-11039; RRID:AB_2534096
Alexa 594 anti-rat	Fisher Scientific	Cat#A11007; RRID:AB_141374
Alexa 647 anti-rabbit	Fisher Scientific	Cat#A21244; RRID:AB_2535812
Chemicals, peptides, and recombinant proteins		
Tamoxifen	Fisher Scientific	Cat#AAJ6350903; CAS#10540–29-1
Experimental models: Organisms/strains		
Mouse: *Wnt1*^{Cre}	Jackson labs	Cat#022137; RRID:IMSR_JAX:022137
Mouse: *Ret*^{CreERT2}	Luo et al.[46]	MGI:4437245
Mouse: *Ntrk3*^{CreERT2}	Jackson labs	Cat#030291; RRID:IMSR_JAX:030291
Mouse: *VGlut3*^{Cre}	Jackson labs	Cat#028534; RRID:IMSR_JAX:028534
Mouse: *Rosa26*^{Ai95}	Jackson labs	Cat#028865; RRID:IMSR_JAX:028865
Mouse: *Rosa26*$^{mT/mG}$	Jackson labs	Cat#007676; RRID:IMSR_JAX:007676
Mouse: *Tau*^{eGFP}	Jackson labs	Cat#005491; RRID:IMSR_JAX:005491
Software and algorithms		
Fiji (ImageJ)	Schindelin et al.[65]	https://imagej.net/Fiji
Cell Magic Wand	Theo Walker	https://github.com/fitzlab/CellMagicWand
LasX	Leica	N/A
Adobe Photoshop 2020	Adobe	N/A
Adobe Illustrator 2020	Adobe	N/A
Prism 9	Graphpad	N/A
Ocular	Teledyne Photometrics	N/A

REAGENT or RESOURCE	SOURCE	IDENTIFIER
pCLAMP Software Suite	Molecular Devices	N/A
Matlab R2019b	MathWorks	N/A
NoRMCorre	Pnevmatikakis and Giovannucci[66]	https://github.com/fiatironinstitute/NoRMCorre
Neuropil extraction	Ghitani et al.[67]	N/A
Clustering Ca Imaging	This paper	https://github.com/GerlingTouchLab/clustering_Ca_imaging; https://doi.org/10.5281/zenodo.6829200
In vivo trigeminal pipeline	This paper	https://github.com/LumpkinLab/invivo_TG_pipeline; https://doi.org/10.5281/zenodo.7135556